This work was carried out in whole or in part within the framework of the NOMATEN Center of Excellence, supported from the European Union Horizon 2020 research and innovation programme (Grant Agreement No. 857470) and from the European Regional Development Fund via the Foundation for Polish Science International Research Agenda PLUS programme (Grant No. MAB PLUS/2018/8).

This is a copy of the publication which appeared in: Surface & Coatings Technology, volume 393 (2020) 125833, published on: 24 April 2020.

DOI: 10.1016/j.surfcoat.2020.125833

Surface & Coatings Technology 393 (2020) 125833

Contents lists available at ScienceDirect

Surface & Coatings Technology

journal homepage: www.elsevier.com/locate/surfcoat

Nanomechanical properties of low-energy Fe-ion implanted Eurofer97 and pure Fe

M. Clozel[a,*], L. Kurpaska[a], I. Jóźwik[a,b], J. Jagielski[a,b], M. Turek[c], R. Diduszko[a,b], E. Wyszkowska[a]

[a] National Centre for Nuclear Research, A. Sołtana str. 7, 05-400 Otwock–Świerk, Poland
[b] Institute of Electronic Materials Technology, Wołczynska str. 133, 01-919 Warsaw, Poland
[c] Institute of Physics, Maria Curie-Skłodowska University, M. Curie-Skłodowskiej pl. 1, 20-031 Lublin, Poland

ARTICLE INFO

Keywords:
Ferritic-martensitic steels
Eurofer97
Pure iron
Ion implantation
Nanoindentation

ABSTRACT

Ferritic-martensitic steels are among the prime candidates to make up structural parts of new generation reactors. Nanoindentation was conducted on 2 materials: low activation Fe-9Cr-1WVTa (Eurofer97) and a model pure iron. Both materials were implanted at low energy (275 keV) with Fe ions at different temperatures (room-temperature, 300 °C, 450 °C), with damage levels ranging from 0.1 to 10 dpa. After implantation, the samples were indented with a diamond Berkovitch tip at room-temperature. The results display varying softening and hardening effects depending on damage level and implantation temperature, which have been correlated with: (i) dislocation loop type distribution, (ii) Cr-content and (iii) the presence of other alloying elements. Obtained mechanical and structural results were compared with the available data from the literature.

1. Introduction

Faced with the reality of climate change, human societies are in dire need of solutions to reduce the production of greenhouse gases, especially in the energy sector. Unlike other sustainable sources of energy such as windmills or photovoltaics, nuclear power provides a stable energy supply. Despite having been left aside for a few years, nuclear energy has once again become attractive, as most of the countries of the world have agreed to sufficiently reduce greenhouse gas emissions to slow and hopefully reverse climate change. This has driven renewed financial support not only of new versions of tested designs (PWRs) but also of new nuclear technologies and concepts – such as the generation IV fission reactors and fusion reactors, which aim to offer better efficiency [1,2].

However, these high-tech reactors require harsher operation conditions in comparison to the previous III generation, such as higher temperatures, higher irradiation levels of the structural materials, and for some, the presence of highly corrosive media like bismuth-lead, molten salt or sodium [1–3]. These conditions make the development of new materials for structural components necessary, and this itself requires the full understanding of the processes, phenomena, and physical mechanisms that occur during irradiation at different temperatures.

Among leading candidates for use in these future reactors, ferritic-martensitic steels show reasonably good thermo-physical and mechanical properties, reduced radiation-induced swelling and helium embrittlement under (fission) neutron irradiation and generally good compatibility with cooling and breeding materials [4–6]. However, they display problematic irradiation-induced embrittlement at temperatures below 350 °C, and loss of creep strength above 550 °C [4–6]. To be able to guarantee (as much as realistically possible) the application of these materials in the GenIV fission and fusion reactors, it is absolutely necessary to improve their properties outside of this temperature frame. For this reason, the objective of this work is to better understand the radiation-induced microstructure of ferritic/martensitic steels and its impact on the mechanical properties and to help screen potential material compositions to be used in future fission and fusion nuclear reactors.

Because neutron irradiation is a time-consuming process (reaching even low dpa levels may require years), it is common to imitate it by using the quicker process of ion implantation, allowing scientists to reach high dpa levels within hours [7]. This process also allows more freedom in the irradiation parameters (energy, fluence, dose rate, ambient temperature), helping in the screening of candidate materials. Usually, self-ion implantation (using the irradiated sample's majority component) is employed to best imitate the damage induced by fast neutrons, while limiting changes in the chemical composition and in

* Corresponding author.
E-mail addresses: Melanie.clozel@ncbj.gov.pl (M. Clozel), Lukasz.kurpaska@ncbj.gov.pl (L. Kurpaska), Iwona.jozwik@ncbj.gov.pl (I. Jóźwik), Jacek.jagielski@ncbj.gov.pl (J. Jagielski), mturek@kft.umcs.lublin.pl (M. Turek), Ryszard.Diduszko@itme.edu.pl (R. Diduszko), Edyta.wyszkowska@ncbj.gov.pl (E. Wyszkowska).

https://doi.org/10.1016/j.surfcoat.2020.125833
Received 14 November 2019; Received in revised form 16 April 2020; Accepted 21 April 2020
Available online 24 April 2020

the type of created defects. Because ion irradiation typically only penetrates from several tens of nanometres to several micrometres into the material, traditional mechanical testing techniques, such as traditional uniaxial tests (e.g. tensile tests) on standard sized samples, are not adapted. However, some works on ion-irradiated micro-pillars do exist [8], and maybe this technique is the future of these tests.

Nanoindentation has become a pervasive technique in the micro- and nanomechanical realms thanks to its sensitivity and broad application area (testing of thin films, coatings, single grains, grain boundaries, different phases, etc.), be it at room-temperature or at elevated temperatures [8–16]. It consists in pressing a nano-scaled hard object (a diamond pyramid, for example) into a material and measuring the material response, allowing an evaluation of both the elastic and the plastic properties of the material. This technique is also known as depth-sensing indentation (DSI) or instrumented indentation testing (IIT), because the contact area is not estimated optically like in macro-scale hardness measurements [16].

If the ion-irradiated layer of a material is treated as analogous to a coating, nanoindentation is an evident choice for the evaluation of its mechanical properties, and indeed, it is often used in this case [11,12,15–21].

This works purports to help understand the processes and phenomena at play in the changes in hardness of ferritic-martensitic steels after Fe-ion implantation, at ambient temperature as well as elevated temperatures.

2. Material and methods

2.1. Materials

Eurofer97 (Fe-9Cr-1WVTa) is one such ferritic-martensitic candidate material [22–27], produced by Böhler Edelstahl AG. Eurofer97's microstructure was obtained by normalising at 1250 K for 27 min followed by air quenching, and tempering at 1030 K for 90 min. The pure Fe was produced by OCAS NV, by casting and hot-rolling immediately after annealing at 930 K for 90 min. Their chemical compositions are provided in Table 1. The samples – plates of dimensions approx. 10 mm × 10 mm, 1 mm thickness – were received from the Joint Research Centre (Eurofer97) and from the Helmholtz Zentrum Dresden-Rosendorf (model iron – reference sample).

2.2. Sample preparation

The sample surfaces were all ground and polished on a MetaServ 250 (BUEHLER) in the following order: SiC grinding papers, from 600 down to 1200 grit, followed by diamond suspensions, from 9 μm down to 3 μm particle size, followed by the final polishing fluid – MasterPolish 0.05 μm (BUEHLER). Later, grinding papers with finer grit were purchased, with the aim of comparing the effects of different polishing techniques on the hardness profiles (such as the ones presented in Fig. 4). When a sample was repolished for subsequent nanoindentation, it was done using P4000 grit grinding paper after the 1200 grit, making the 9 μm and 6 μm polishing phases unnecessary. This yielded a sample with less surface strain.

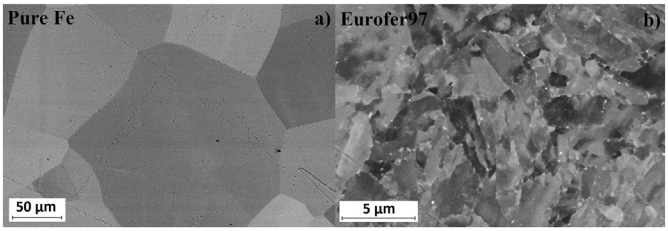

Fig. 1. Microstructures of a) pure Fe, b) Eurofer97 - Fe-9Cr-1WVTa.

The microstructures of pure iron and Eurofer97 are shown in Fig. 1. The pure iron (Fig. 1 a)) presents large grains with an average size of 95 μm. It should be pointed out that the scale is 10 times smaller for Eurofer97 (Fig. 1 b)), whose ferritic-martensitic microstructure presents – in addition to its large density of grain boundaries – carbides (MC, $M_{23}C_6$) [26,27] dispersed on the grain boundaries and in the grains.

2.3. Ion implantation

After reaching a satisfactory surface aspect, implantations were performed according to the parameters presented in Table 2 using an UNIMAS 79 ion implanter at Institute of Physics, Maria Curie-Skłodowska University in Lublin, Poland, equipped with arc discharge plasma ion source with internal evaporator [28,29]. Iron (III) chloride was used as a feeding substance that was placed into a large size evaporator [30] partially inserted into the ion source chamber. Irradiations with 275 keV Fe^+ ions were done with fluences up to 3.5×10^{13}, 3.5×10^{14} and 3.5×10^{15} ions/cm^2, which is equivalent to 0.1, 1 and 10 dpa, respectively. Ion current density at the target was ≈100 nA/cm^2. The implantation campaign was performed at room temperature and at elevated temperatures (300 °C or 450 °C), for which the sample holder was equipped with a HTR1002 heater (Boralectric, Momentive, Strongsville OH, USA). In the interest of comparison between the effects of neutron and ion irradiation, the parameters of implantation temperature and damage levels were chosen to mimic conditions in the most commonly operated pressurised water reactor type nuclear reactors (temperatures up to circa 350 °C, damage levels of structural materials up to several dpa). The pressure inside the target chamber was maintained at vacuum-like conditions (≈10^{-6} mbar) during the whole procedure. The implantation current density was kept at 100 nA/cm^2 with intermittent faults no larger than 10% as observed by using current integrator display. The long run current drift was corrected by discharge and cathode filament currents as well as beam scan voltage adjustments. The vacuum in the ion duct and the sample chamber was provided by turbo-molecular pumps used in order to prevent carbon deposition onto the sample surface. No signs of carbon deposition were detected during multiple test (performed e.g. at Helmholtz-Zentrum Dresden-Rosendorf) of various samples implanted using Lublin implanter. The sample chamber is insulated from the rest of the device and connected to RRAJ implantation current integrator based on the current-frequency converter. The precision of the current integrator (and hence the implantation fluence error) is below 1% - confirmed by SIMS measurements e.g. for Al and Be implantations - matched within SIMS

Table 1
Chemical compositions.

	Cr	Mo	Mn	Si	V	Ni	Nb	Cu	Al
Eurofer97	8.87	0.001	0.42	0.06	0.19	0.0075	< 0.001	0.021	0.008
Pure Fe	0.002	< 10 ppm	< 10 ppm	0.001	< 10 ppm	0.007	< 10 ppm	< 10 ppm	0.023
	C	N	P	S	Sn	O	W	Ta	Ti
Eurofer97	0.12	0.018	0.004	0.003	< 0.005	0.001	1.1	0.14	0.008
Pure Fe	< 0.005	< 10 ppm	0.003	10–15 ppm	< 10 ppm	< 10 ppm	< 10 ppm	< 10 ppm	< 10 ppm
	Co	As	Sb	Zr					
Eurofer97	0.005	< 0.005	< 0.005	< 0.005					
Pure Fe	≈50 ppm	< 10 ppm	< 10 ppm	< 10 ppm					

Table 2
Implantation parameters at room temperature, 300 °C, and 450 °C. The "x" mark the irradiations performed.

Provider	Material	Damage [dpa]	Fluence [ions/cm^2]	Ion	Energy [keV]	Implantation temperature [°C]		
						25	300	450
JRC (BOEHLER)	Eurofer97	0	0	Fe^+	275	x	x	x
		0.1	3.10E+13			x	x	x
		1	3.10E+14			x	x	x
		10	3.10E+15				x	x
HZDR	Pure Fe	0	0	Fe^+	275	x		
		0.1	3.10E+13				x	x
		1	3.10E+14				x	

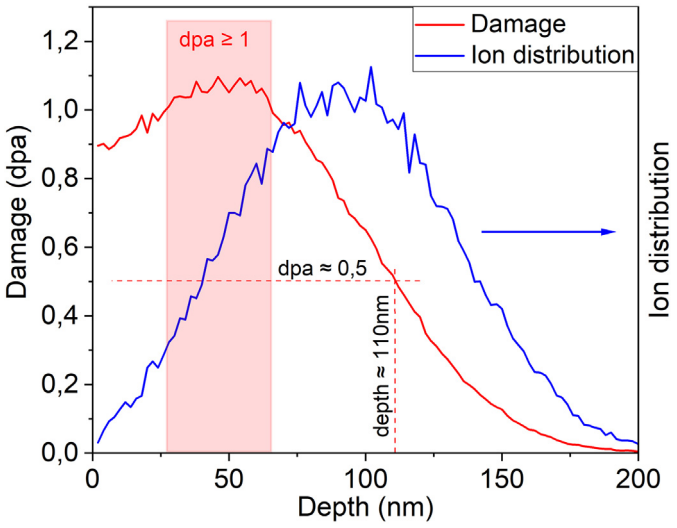

Fig. 2. dpa profile and ion distribution of Fe ions in Fe at 275 keV and a fluence of 3.50 × 10^{14}.

accuracy.

The produced damage profiles at room temperature were calculated from the energy from ions results obtained through simulation in SRIM2008 (see example for 1 dpa in Fig. 2), using the following equation:

$dpa = \frac{E_i}{2 \cdot E_d} \cdot \Phi \cdot V_a$, where E_i is the energy from ions, E_d is the displacement energy, Φ is the fluence, and V_a is the atomic volume. In agreement with [31], 40 eV is chosen for E_d (the displacement energy). The atomic volume of iron is 11.77 Å^3 (calculated from the molar volume and the Avogadro constant). The fluence 3,50 × 10^{14} ions/cm^2 is shown as an example in Fig. 2. As can be seen on the graph, the damage profile is not constant, so that the 1 dpa level is only absolutely valid between 25 and 65 nm (see the greyed-out square in Fig. 2). If we are to limit nanoindentation depths to a tenth or a fifth of the damaged layer, this would mean targeting depths between 6 and 13 nm. However, because of technical constraints (limited force and depth resolution of the nanoindentation devices, vibratory noise, thermal disparities, as well as surface roughness), reliable results can hardly be obtained at these depths. If it is assumed that the damaged layer is circa 110 nm thick (the depth for half the maximum dpa, see blue line in Fig. 2), the mechanical response with nanoindentation depths ranging from 11 to 22 nm is expected to be mostly from this damaged layer. However, the surface preparation was later found to be imperfect for nanoindentations at these depths, so that the produced results may be burdened with an influence of the surface quality (i.e. roughness and strains). In the continuation of this work, electropolishing and ion implantation campaigns with higher energy will help alleviate these issues.

2.4. Nanoindentation

Nanoindentation was performed on the NanoTest Vantage systems (MicroMaterials Ltd.) in NCBJ, with a diamond Berkovitch indenter. Depths ranging from circa 12 nm to around 1 μm were measured with loads ranging from 0.05 mN to 50 mN. Measuring the hardness or modulus as a function of depth on the virgin samples allows the observation of the surface effects, such as surface preparation and Indentation Size Effect (ISE, described later) [32–38], so that when measuring the irradiated samples, the influence of irradiation can be – at least to a certain extent – separated from these surface effects. Besides limiting the surface roughness when using nanoindentation, it is also important to limit as much as possible the thermal disparity between the sample and the indenter, because this difference can lead to changes of the order of several nanometres to tens of nanometres in the depth measurements (the reader should remember that the range of the nanoindentation depths reached starts from approx. 12 nm). A thermostat and a small heater are used within the indentation chamber to keep it at a constant temperature (approximately 1° above actual room temperature). The roundedness of the indenter tip, the Diamond Area Function (DAF) of the indenter is deduced from indentation results of a calibration sample (fused silica).

Nanoindentations were performed following the typical load profiles as presented in Fig. 3 (load vs. time and load vs. depth, respectively). 20 indents are performed for the smaller loads (0.05 mN to 0.7 mN), 15 indents for the intermediate loads (1 mN to 2 mN), and finally 10 indents for the higher loads (5 mN to 50 mN). For loads ranging from 0.05 mN to 2 mN, loading, holding, and unloading times were set to 5 s, 1 s, 3 s, respectively. For loads ranging from 5 mN to 50 mN, loading, holding, and unloading times were set to 10 s, 2 s, 5 s, respectively. The 60 s thermal drift measurement at the end of the indentation is done to measure the thermal disparity between the sample and the indenter. A correction can then be applied based on this measurement, when analysing the results.

3. Results

Fig. 4 shows hardness profiles from single-cycle indents. The hardness increase at shallower depths is mostly due to what is commonly known as Indentation Size Effect (ISE) [32–38]. This effect is produced when the average space between dislocations is on par with the volume sampled with the indenter, and endures until a certain ratio of indent size over grain size, after which the hardness becomes constant [36]. ISE is visible for both materials shown in this report. With the hardness profiles for unirradiated samples available, it was hoped that the irradiated samples could be indented and their results compared, so as to observe the effects of temperature and damage levels on the mechanical properties. In Fig. 4, the first results of the pure iron and the Eurofer97 samples are presented. In Fig. 4 a), the pure iron shows a noticeable increase in hardness after irradiation at 0.1 dpa at 300 °C, but almost returns to the unirradiated hardness when irradiated at 450 °C. Furthermore, the hardness of the unimplanted pure iron samples is

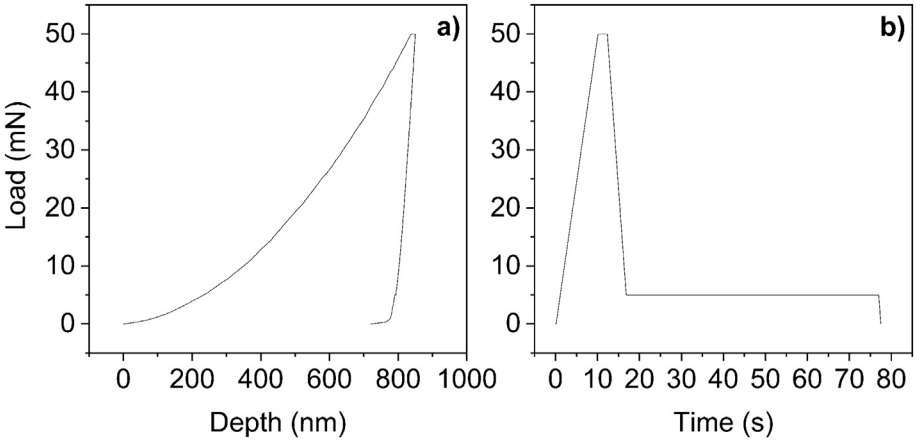

Fig. 3. (a) Typical load vs time profile for room-temperature nanoindentation (example at 50 mN), (b) typical load vs depth profile for nanoindentation (example at 50 mN).

constant enough to assume that no hard oxide appeared on the specimen surface during implantation at high temperature. For Eurofer97, after irradiation at 1 dpa, the sample displayed no difference in hardness with the unirradiated state, whereas irradiation at 10 dpa caused a noticeable increase, see Fig. 4 b). Even if the results from the first 200 nm of the surface (greyed-out areas in Fig. 4) are removed because of possible surface preparation influence, there is still hardening with higher irradiation damage, and softening from higher irradiation temperatures. Furthermore, it was observed using an optical microscope on irradiated Fe−9Cr samples that the higher damage levels make the polycrystalline structure of the material more visible as a result of preferential sputtering: depending on the grain orientation, the ion beam cause more or less sputtering, creating different levels at the surface. The grains were also visible to a certain extent in the hardness measurements, as some grain-orientations seem to provide greater resistance to indentation, causing higher disparity in the results. The literature provides an example of the grain-orientation dependence of helium-implanted tungsten [9], another BCC-structured alloy, where the authors conclude that the "significantly different indentation behaviour […] observed for different grain orientations in the implanted material highlights the importance of considering crystal orientation when interpreting nanoindentation data".

As it became clear that different hardness profile results were obtained depending on the indent positions, with respect to grain boundaries and grain orientations, it was decided to perform more indentations than the typical 10–20 indents. Therefore, "maps" of 7 × 7 to 10 × 10 indents were performed at load 0.3 mN (where the peak in the hardness profile appeared for most samples). This provided more realistic average hardness results. Fig. 5 presents the results from these later mappings. Results are displayed for three irradiation temperatures – 25 °C, 300 °C, and 450 °C – in unirradiated state and irradiated to 0.1 dpa.

Because only 5 samples of pure Fe were available in total, after all measurements were performed on the two pure iron samples irradiated to 0.1 dpa at 300 °C and at 450 °C, these two samples were polished down so as to have an equivalent 0 dpa (unirradiated, but after ageing at 300 and 450 °C, respectively).

Based on the presented data, the following observations can be made:

- Starting from the pure iron (Fig. 5 a)), a large increase in hardness is observed whatever the irradiation damage and temperature. The hardness is slightly lower at 450 °C compared to 300 °C, and in Fig. 5 c), the reduced modulus is slightly lower at 0.1 dpa than in the unirradiated condition.
- The Eurofer97 sample (Fig. 5 b)) displays an increase in hardness at 0.1 dpa. For this material, implanting at different temperatures does not seem to affect the implantation-induced hardness. In Fig. 5 d), the reduced modulus decreases slightly whatever the implantation temperature.

4. Discussion

Surface preparation is vitally important in obtaining reliable results. The hardness value for pure Fe virgin at room-temperature was initially over 4 GPa, higher than Eurofer97, which was simply due to surface preparation. P4000 grinding paper was obtained after the initial nanoindentation runs. Samples repolished with this paper (followed by

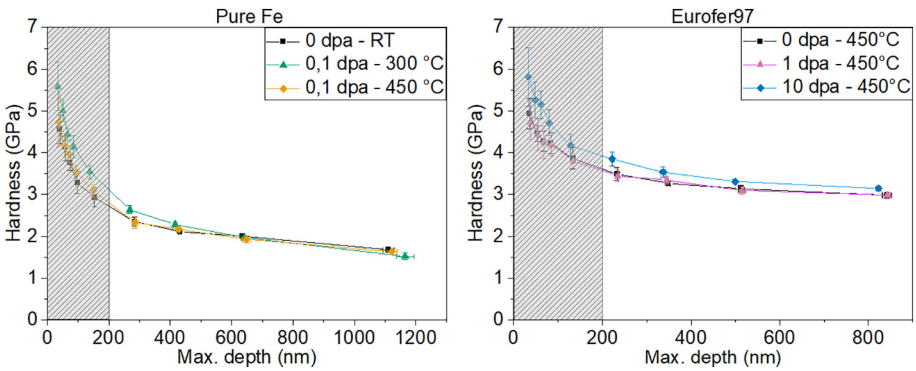

Fig. 4. Hardness profiles of pure Fe in unirradiated state, irradiated to 0.1 dpa at 300 °C and 450 °C (left), and Eurofer97 irradiated at 450 °C at different dpa levels (right).

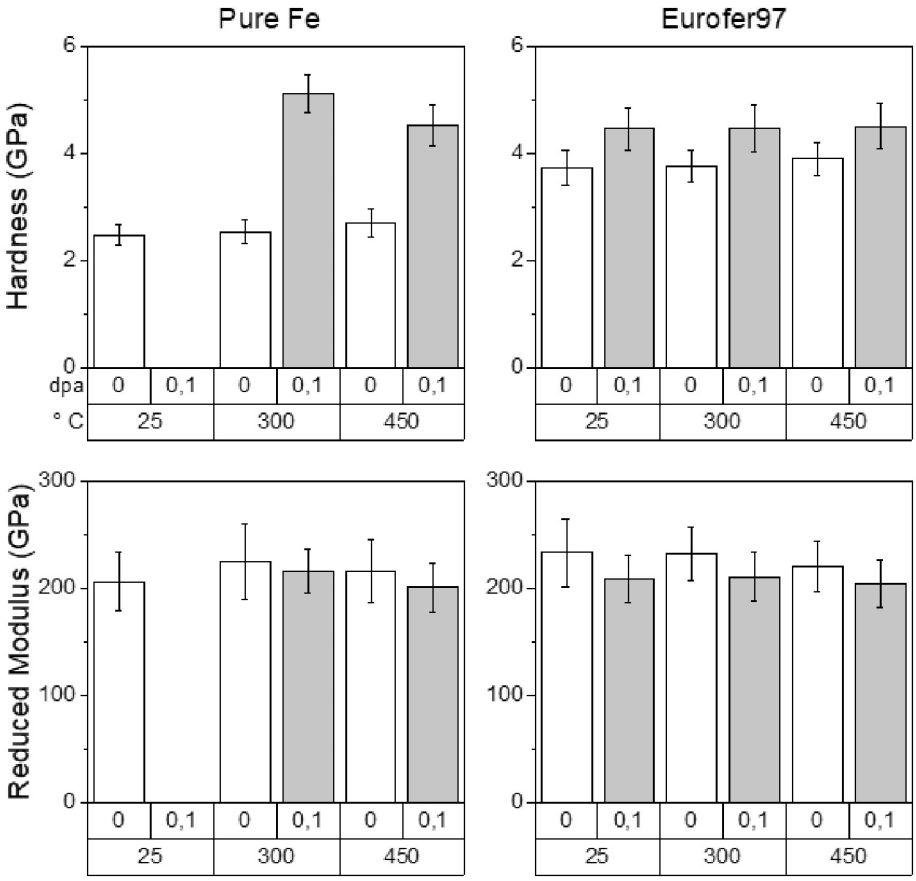

Fig. 5. Hardness and reduced modulus results at 0.3 mN of pure Fe and Eurofer97, after irradiation at 25 °C, 300 °C, 450 °C, with 0 dpa and 0.1 dpa.

diamond pastes and the final polishing fluid) provided the expected (lower) hardness results, indicating less strain induced by the grinding and polishing. For this reason, it is difficult to say in the irradiated samples, how much of the hardening is due to surface preparation, especially in pure Fe irradiated samples. This will be repeated in future studies.

Using Positron Annihilation Spectrometry, Atomic Probe Tomography, and TEM studies, it was found [20,39–43] that for Fe, Fe—Cr and Fe-Cr-NiSiP alloys, and in the case of irradiations equal to or above ambient temperature:

- The higher the irradiation temperature, the lower the concentration in vacancy-defects and their size (at 450 °C, the concentration in vacancy-defects after 0,5 dpa irradiation was too low to be detected).
- At T_{irr} = 300 °C, the higher the dpa, the lower the concentration in vacancy-defects and their size, and the higher the dislocation concentration.
- At T_{irr} = 300 °C, the higher the impurities content, the higher the concentration in vacancy defects, the smaller the dislocation loops, the more solute rich clusters (SRC) (and the lower their size), and the richer these clusters are in Cr and impurities.
- At any given T_{irr}, the higher the impurity content, the harder the material.

From our results and the points presented above, we can make the following hypotheses:

- The hardening in pure Fe is probably due to vacancy-defects, decreasing in density at higher temperature so that the irradiation-induced hardening decreases also, and dislocations, which should increase in density with dpa. There should be no or very few solute rich clusters.
- As the conclusions from the literature mentioned previously [20,39–43] apply only to Fe, Fe—Cr and Fe-Cr-NiSiP, only an initial extrapolation can be made about Eurofer97 (Fe-9Cr-1WVTa). Its hardening may be due to the same defects as Fe-9CrNiSiP, but with more SRC, as there are more alloying elements, and more variety in those elements. The grains are also a lot smaller, by around 2 orders of magnitude, which means there are a lot more grain boundaries. This will undoubtedly affect the dislocation movement and the diffusion process, as grain boundaries are preferential diffusion routes for point defects [44,45] because of the lower atom packing density, especially at higher temperature. The hardness at 0.1 dpa is approximately irradiation temperature independent. This would imply that vacancy-defects are not the main cause of hardening at 0.1 dpa. At 10 dpa, the hardness increases with temperature, so that one can expect that the main cause of hardening may be due to SRC (by increasing diffusion of solute atoms).

Because these explanations apply to higher energy implantation, it is possible that different phenomena interact in the specimens studied in this work. Of course, effects from the surface preparation and the indentation curves analysis cannot be completely excluded. TEM analysis would be necessary to help determine the reason for this divergence. Results for ion irradiation hardening of Eurofer97 are available in the literature. According to Heintze et al. [43,46], the hardening for this sample after irradiation at 300 °C to 1 dpa is in the range of 0.25 to 0.75 GPa. The hardening observed in this work for 0.1 dpa at 300 °C is 0.7 GPa. It would be expected for Eurofer97 to display less hardening at this low dose. However, the results mentioned from the literature were caused by high-energy implantation, so that it is possible that the low-

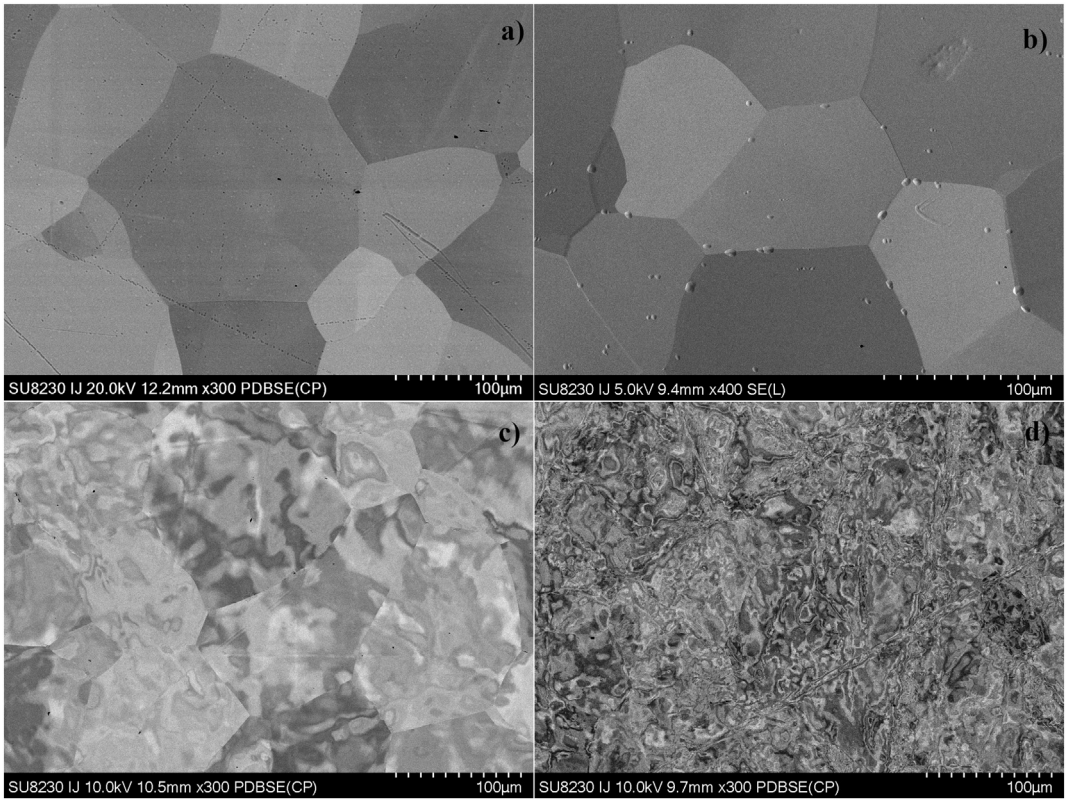

Fig. 6. SEM micrographs in virgin state of pure Fe, a) at room-temperature, b) after ageing at 300 °C, c) after ageing at 450 °C, d) after ageing at 600 °C.

energy implantation causes different microstructural damage. This will be examined with TEM in the upcoming work. The literature [39] does provide TEM micrographs of pure Fe before and after ion irradiation with 5 MeV Fe ions. After irradiation, dark dots are visible, identified as dislocation loops and solute rich clusters (SRC).

Until now, the effect of temperature on the microstructure was not broached. In Fig. 6, SEM micrographs can be found (in this case, backscattering electrons after ion-beam polishing) of the microstructure of pure Fe in as-received state (Fig. 6 a)), and after ageing at 300 °C (Fig. 6 b)), 450 °C (Fig. 6 c)) and 600 °C (Fig. 6 d)). No change is visible at 300 °C, however at higher temperatures, there seems to be significant change in the lattice strains, so that each grain presents many local lattice orientations. This was confirmed with XRD measurements of the same samples (see Appendix A, Table 3). Apart from being aesthetically appealing, Fig. 6 shows that the difference in hardness for pure Fe at 450 °C is not solely due to irradiation effects. Similar research will be performed on Eurofer97.

5. Conclusion

Irradiation to 0.1 dpa causes an increase in hardness in both samples for all implantation temperatures. As the temperature increases however, less hardening is visible in the case of pure iron, but this effect is not observed in Eurofer97, where the hardening seems temperature independent. These results find justification in the literature, although there are some differences, likely due to the low implantation energies employed for this work, and to the polishing quality. The hardening in pure iron is likely due to vacancy-defects, the fraction of which would be reduced as the temperature increases. Additionally, some purely thermal effects on the microstructure of pure iron were observed: the higher the temperature, the more strained the lattice. Eurofer97, on the other hand, presents a higher initial hardness because of the large presence of alloying elements, as well as much smaller grains, and therefore, higher fraction of grain-boundaries. The hardening in Eurofer97 with irradiation is probably due to dislocation loops and solute-rich clusters. The fact that the temperature does not seem to

Table 3
XRD analysis results of pure iron after ageing at ambient temperature, 300 °C, 450 °C, and above 600 °C.

		Pure Fe, aged at RT	Pure Fe, aged at 300 °C	Pure Fe, aged at 450 °C	Pure Fe, aged at 600 °C
Lattice parameters	Method	WPPF	WPPF	WPPF	WPPF
	a(Å)	2.86699(5)	2.86678(7)	2.86740(4)	2.86767(10)
	b(Å)	2.86699(5)	2.86678(7)	2.86740(4)	2.86767(10)
	c(Å)	2.86699(5)	2.86678(7)	2.86740(4)	2.86767(10)
	alpha(°)	90	90	90	90
	beta(°)	90	90	90	90
	gamma(°)	90	90	90	90
	V(Å^3)	23.5655(7)	23.5605(11)	23.5756(6)	23.5823(14)
Quantitative value	Method	WPPF	WPPF	WPPF	WPPF
	Value (%)	100	100	100	100
Crystallite size	Value (Å)	975(3)	663.3(18)	479.2(11)	452.3(13)
Strain		0.0196(16)	0.0356(17)	0.0554(19)	0.040(4)

affect the hardness of this material tends to highlight that the hardening is not due to vacancy-defects.

Credit author statement

Mélanie Clozel: Methodology, Investigation, Validation, Formal Analysis, Writing – Original Draft, Visualization

Łukasz Kurpaska: Conceptualization, Methodology, Supervision, Writing – Review and Editing

Iwona Jóźwik: Investigation

Jacek Jagielski: Conceptualization

Ryszard Diduszko: Investigation

Edyta Wyszkowska: Investigation

Declaration of competing interest

The authors declare that they have no known competing financial interests or personal relationships that could have appeared to influence the work reported in this paper.

Acknowledgements

Funding: This work was supported by the Euratom research and training programme 2014-2018 under grant agreement no. 755039 (M4F project) and has been supported by the EURATOM Direct Actions.

This work also contributes to the Joint Programme on Nuclear Materials (JPNM) of the European Energy Research Alliance (EERA).

The authors would like to thank Dr. Bergner and Dr. Heintze for their helpful explanations.

Appendix A. XRD analysis

It was not possible to set the beam in such a way that it covered only the surface of the samples, so that there is always an additional signal from the epoxy in which the samples were embedded, and sometimes also a trace from the steel mounting springs. The diffractograms show four reflections from Fe (bcc structure): 110, 200, 211 and 220. The first, strongest reflex was unfortunately disturbed by the mounting springs, so that it was not included in the analysis. From the remaining three reflections, the Rietveld method was used to calculate structure parameters - it can be seen in Table 3 that as the temperature increases, the average size of crystallites decreases and the strain parameter increases. The network constant increases slightly (almost at the limit of error).

References

[1] T.R. Allen, J.T. Busby, M. Meyer, D. Petti, Materials challenges for nuclear systems, Mater. Today 13 (2010) 14–23.
[2] S.J. Zinkle, J.T. Busby, Structural materials for fission & fusion energy, Mater. Today 12 (2009) 12–19.
[3] NERAC, A Technology Roadmap for Generation IV Nuclear Energy Systems, (2002).
[4] R.L. Klueh, A.T. Nelson, Ferritic/martensitic steels for next-generation reactors, J. Nucl. Mater. 371 (2007) 37–52.
[5] G.S. Was, J.P. Wharry, B. Frisbie, B.D. Wirth, D. Morgan, J.D. Tucker, T.R. Allen, Assessment of radiation-induced segregation mechanisms in austenitic and ferritic–martensitic alloys, J. Nucl. Mater. 411 (2011) 41–50.
[6] A. Kohayama, A. Hishinuma, D.S. Gelles, R.L. Klueh, W. Dietz, K. Ehrlich, Low-activation ferritic and martensitic steels for fusion application, J. Nucl. Mater. (1996) 138–147.
[7] Y. Wu, Fusion Neutronics, Springer Berlin Heidelberg, New York NY, 2017.
[8] J.R. Greer, J.T.M. de Hosson, Plasticity in small-sized metallic systems, Prog. Mater. Sci. 56 (2011) 654–724.
[9] S. Das, H. Yu, E. Tarleton, F. Hofmann, Orientation-dependent indentation response of helium-implanted tungsten, Appl. Phys. Lett. 114 (2019) 221905.
[10] S.A. Syed Asif, J.B. Pethica, Nano-scale indentation creep testing at non-ambient temperature, J. Adhesion 67 (1998) 153–165.
[11] C.D. Hardie, S.G. Roberts, A.J. Bushby, Understanding the effects of ion irradiation using nanoindentation techniques, J. Nucl. Mater. 462 (2015) 391–401.
[12] C.D. Hardie, S.G. Roberts, Nanoindentation of model Fe–Cr alloys with self-ion irradiation, J. Nucl. Mater. 433 (2013) 174–179.
[13] M.L. Oyen, R.F. Cook, A practical guide for analysis of nanoindentation data, J. Mech. Behav. Biomed. Mater. 2 (2009) 396–407.
[14] J.M. Wheeler, D.E.J. Armstrong, W. Heinz, R. Schwaiger, High temperature nanoindentation: the state of the art and future challenges, Curr. Opin. Solid State Mater. Sci. 19 (2015) 354–366.
[15] J.S.K.-L. Gibson, S.G. Roberts, D.E.J. Armstrong, High temperature indentation of helium-implanted tungsten, Mater. Sci. Eng. A 625 (2015) 380–384.
[16] A.C. Fischer-Cripps (Ed.), Nanoindentation, 2nd ed., Springer, New York, London, 2004.
[17] B. Duan, C. Heintze, F. Bergner, A. Ulbricht, S. Akhmadaliev, E. Oñorbe, Y. de Carlan, T. Wang, The effect of the initial microstructure in terms of sink strength on the ion-irradiation-induced hardening of ODS alloys studied by nanoindentation, J. Nucl. Mater. 495 (2017) 118–127.
[18] A. Lupinacci, K. Chen, Y. Li, M. Kunz, Z. Jiao, G.S. Was, M.D. Abad, A.M. Minor, P. Hosemann, Characterization of ion beam irradiated 304 stainless steel utilizing nanoindentation and Laue microdiffraction, J. Nucl. Mater. 458 (2015) 70–76.
[19] C. Heintze, F. Bergner, S. Akhmadaliev, E. Altstadt, Ion irradiation combined with nanoindentation as a screening test procedure for irradiation hardening, J. Nucl. Mater. 472 (2016) 196–205.
[20] C. Heintze, F. Bergner, M. Hernández-Mayoral, Ion-irradiation-induced damage in Fe–Cr alloys characterized by nanoindentation, J. Nucl. Mater. 417 (2011) 980–983.
[21] P. Hosemann, C. Vieh, R.R. Greco, S. Kabra, J.A. Valdez, M.J. Cappiello, S.A. Maloy, Nanoindentation on ion irradiated steels, J. Nucl. Mater. 389 (2009) 239–247.
[22] F. Bergner, G. Hlawacek, C. Heintze, Helium-ion microscopy, helium-ion irradiation and nanoindentation of Eurofer 97 and ODS Eurofer, J. Nucl. Mater. 505 (2018) 267–275.
[23] E. Materna-Morris, A. Möslang, H.-C. Schneider, Tensile and low cycle fatigue properties of EUROFER97-steel after 16.3dpa neutron irradiation at 523, 623 and 723K, J. Nucl. Mater. 442 (2013) S62–S66.
[24] S. Knitel, Investigations and numerical modeling of mechanical properties of tempered martensitic steel Eurofer97 at various loading rates, temperatures and after spallation irradiation, Suisse, 2018. https://infoscience.epfl.ch/record/255179, consulted 08-nov-2019.
[25] A.-A.F. Tavassoli, A. Alamo, L. Bedel, L. Forest, J.-M. Gentzbittel, J.W. Rensman, E. Diegele, R. Lindau, M. Schirra, R. Schmitt, H.C. Schneider, C. Petersen, A.-M. Lancha, P. Fernandez, G. Filacchioni, M.F. Maday, K. Mergia, N. Boukos, Baluc, P. Spätig, E. Alves, E. Lucon, Materials design data for reduced activation martensitic steel type EUROFER, J. Nucl. Mater. 329-333 (2004) 257–262.
[26] M. Matijasevic, E. Lucon, A. Almazouzi, Behavior of ferritic/martensitic steels after n-irradiation at 200 and 300°C, J. Nucl. Mater. 377 (2008) 101–108.
[27] P. Fernández, A.M. Lancha, J. Lapeña, M. Hernández-Mayoral, Metallurgical characterization of the reduced activation ferritic/martensitic steel Eurofer'97 on as-received condition, Fusion Eng. Des. 58-59 (2001) 787–792.
[28] M. Turek, S. Prucnal, A. Droździel, K. Pyszniak, Versatile plasma ion source with an internal evaporator, Nucl. Instrum. Meth. Phys. Res. Sect. B 269 (2011) 700.
[29] M. Turek, A. Droździel, K. Pyszniak, S. Prucnal, Compact hollow cathode ion source with an internal evaporator, Nucl. Instrum. Meth. Phys. Res. Sect. A 654 (2011) 57.
[30] M. Turek, A. Droździel, K. Pyszniak, S. Prucnal, D. Mączka, Yu. Yushkevich, A. Vaganov, Plasma sources of ions of solids, Instrum. Exp. Tech. 55 (2012) 469.
[31] NSC, Primary Radiation Damage in Materials: Review of Current Understanding and Proposed New Standard Displacement Damage Model to Incorporate in Cascade Defect Production Efficiency and Mixing Effects, (2015).
[32] A.A. Elmustafa, D.S. Stone, Indentation size effect in polycrystalline F.C.C. metals, Acta Mater. 50 (2002) 3641–3650.
[33] A.C. Fischer-Cripps (Ed.), Nanoindentation, 2nd ed., Springer, New York, London, 2004.
[34] A.C. Fischer-Cripps, Critical review of analysis and interpretation of nanoindentation test data, Surf. Coat. Technol. 200 (2006) 4153–4165.
[35] T. Zhu, A. Bushby, D. Dunstan, Size effect in the initiation of plasticity for ceramics in nanoindentation, J. Mech. Phys. Solid. 56 (2008) 1170–1185.
[36] X.D. Hou, A.J. Bushby, N.M. Jennett, Study of the interaction between the indentation size effect and hall–Petch effect with spherical indenters on annealed polycrystalline copper, J. Phys. D. Appl. Phys. 41 (2008) 74006.
[37] X. Hou, N.M. Jennett, Application of a modified slip-distance theory to the indentation of single-crystal and polycrystalline copper to model the interactions between indentation size and structure size effects, Acta Mater. 60 (2012) 4128–4135.
[38] A. Ruiz-Moreno, P. Hähner, Indentation size effects of ferritic/martensitic steels: a comparative experimental and modelling study, Mater. Des. 145 (2018) 168–180.
[39] European Commission, Community research, materials' innovations for safe and sustainable nuclear in Europe, Deliverable 2.31: Microstructural and Mechanical Characterisation of Selected Ion and Neutron Irradiated Alloys, Horizon 2020, 2017.
[40] B. Gómez-Ferrer, C. Heintze, C. Pareige, On the role of Ni, Si and P on the nanostructural evolution of FeCr alloys under irradiation, J. Nucl. Mater. 517 (2019) 35–44.
[41] C. Pareige, V. Kuksenko, P. Pareige, Behaviour of P, Si, Ni impurities and Cr in self ion irradiated Fe–Cr alloys – comparison to neutron irradiation, J. Nucl. Mater. 456 (2015) 471–476.
[42] C. Heintze, F. Bergner, M. Hernández-Mayoral, R. Kögler, G. Müller, A. Ulbricht, Irradiation hardening of Fe–9Cr-based alloys and ODS Eurofer, J. Nucl. Mater. 470 (2016) 258–267.
[43] Heintze, C. (2013) Einfluss Der Bestrahlung Mit Energiereichen Teilchen Auf Die Härte Von Fe-Cr-Legierungen. Technischen Universität Dresden, Dresden. Helmholtz-Zentrum Dresden-Rossendorf. http://nbn-resolving.de/

urn:nbn:de:bsz:14-qucosa-120166, consulted 23-apr-2018 – in German.
[44] L.K. Mansur, Theory of transitions in dose dependence of radiation effects in structural alloys, J. Nucl. Mater. 206 (1993) 306.
[45] G.S. Was, Fundamentals of Radiation Materials Science, Second edition, Springer Berlin Heidelberg, Berlin, Heidelberg, 2017.
[46] C. Heintze, C. Recknagel, F. Bergner, M. Hernández-Mayoral, A. Kolitsch, Ion-irradiation-induced damage of steels characterized by means of nanoindentation, Nucl. Instrum. Meth. Phys. Res. Sect. B: Beam Interact. Mater. Atoms 267 (2009) 1505–1508.